Grating interferometry-based phase microtomography of atherosclerotic human arteries

Marzia Buscema[a], Margaret N. Holme[a], Hans Deyhle[a], Georg Schulz[a], Rüdiger Schmitz[a], Peter Thalmann[a], Simone E. Hieber[a], Natalia Chicherova[a,b], Philippe C. Cattin[b], Felix Beckmann[c], Julia Herzen[c,d], Timm Weitkamp[e], Till Saxer[f], and Bert Müller*[a]

[a]Biomaterials Science Center, University of Basel, c/o University Hospital Basel, 4031 Basel, Switzerland; [b]Medical Image Analysis Center, University of Basel, c/o University Hospital Basel, 4031 Basel, Switzerland; [c]Institute of Materials Research, Helmholtz-Zentrum Geesthacht, 21502 Geesthacht, Germany; [d]Physics Department & Institute of Medical Engineering, Technische Universität München, Garching, Germany; [e]Synchrotron Soleil, 91190 Gif-sur-Yvette, France; [f]University Hospitals of Geneva, 1206 Geneva, Switzerland

ABSTRACT

Cardiovascular diseases are the number one cause of death and morbidity in the world. Understanding disease development in terms of lumen morphology and tissue composition of constricted arteries is essential to improve treatment and patient outcome. X-ray tomography non-destructively provides three-dimensional data with micrometer resolution. However, a common problem is simultaneous visualization of soft and hard tissue-containing specimens, such as atherosclerotic human coronary arteries. Unlike absorption-based techniques, where X-ray absorption strongly depends on atomic number and tissue density, phase contrast methods such as grating interferometry have significant advantages as the phase shift is only a linear function of the atomic number. We demonstrate that grating interferometry-based phase tomography is a powerful method to three-dimensionally visualize a variety of anatomical features in atherosclerotic human coronary arteries, including plaque, muscle, fat, and connective tissue. Three formalin-fixed, human coronary arteries were measured using advanced laboratory μCT. While this technique gives information about plaque morphology, it is extremely challenging to extract the lumen morphology from calcified artery specimens. Therefore, selected regions were measured using grating-based phase tomography, sinograms were treated with a wavelet-Fourier filter to remove ring artifacts, and reconstructed data were processed to allow extraction of vessel lumen morphology. Phase tomography data in combination with conventional laboratory μCT data of the same specimen shows potential, through use of a joint histogram, to identify more tissue types than either technique alone. Such phase tomography data was also rigidly registered to subsequently decalcified arteries that were histologically sectioned, although the quality of registration was insufficient for joint histogram analysis.

Keywords: Grating interferometry, stenosed human arteries, synchrotron radiation, wall shear stress, joint histogram, phase tomography, heterogeneous soft and hard tissues, three-dimensional visualization and representation.

1. INTRODUCTION

Cardiovascular diseases refer to any disease that affects the cardiovascular system, principally cardiac disease (including myocardial infarction), vascular disease of the brain (including stroke), kidney disease and peripheral arterial disease. There are many causes of cardiovascular disease, but atherosclerosis and hypertension are most common. Smoking and obesity have been identified as factors in 36 % and 20 % of coronary artery diseases, respectively, lack of exercise in 7 to 12 % of cases and work-related stress for about 3 % of cases [1, 2]. These lead to the alteration of cardiovascular function and, in the worst case, to acute myocardial infarction (AMI). AMI refers mainly to two types of acute coronary syndrome that are often related to coronary artery diseases. The most common occurrence is the rupture of an atherosclerotic plaque, which exposes prothrombotic material from the core of the plaque and leads to an almost or complete occlusion of the artery [3]. In such medical emergencies, vasodilators such as nitroglycerine play a critical role in maintaining blood flow to the tissues supplied by the affected artery. However, the non-specific action of such drugs often leads to dangerous systemic hypotension.

*bert.mueller@unibas.ch; phone +41 61 265 9659; fax +41 61 265 9699; www.bmc.unibas.ch

Developments in X-Ray Tomography IX, edited by Stuart R. Stock, Proc. of SPIE Vol. 9212, 921203 · © 2014 SPIE · CCC code: 0277-786X/14/$18 · doi: 10.1117/12.2060443

It is well known that blood flow due to the local velocity field induces shear stresses along vessel walls [4]. The shear stress is proportional to the viscosity and flow rate, and inversely proportional to the third power of the vessel radius. Therefore, a small decrease in vessel radius can lead to a high increase in local shear stress [5]. Nano-containers formulated from e.g. synthetic phospholipids [6] can be designed to locally release an encapsulated drug above defined shear stress threshold values [7]. This minimizes systemic side effects often seen when injecting e.g. un-encapsulated vasodilators such as nitroglycerine into the vascular system. For localized release of an encapsulated drug from mechano-sensitive nano-containers, an understanding of the shear stresses in healthy and constricted arteries is needed. Quantifying such shear stresses requires the detailed morphology of both healthy and diseased explanted human arteries, which can be used for blood flow simulations.

Micro-computed tomography (μCT) allows non-destructive, quantitative 3D imaging yielding spatial resolution in the 1 to 10 μm scale, which is one to two orders of magnitude higher than in other techniques, such as MRI as seen for human brain [8]. Nevertheless, the 2D spatial resolution is inferior to that of histology, which remains the gold standard for tissue characterization including its function. However, histology has its disadvantages; the resolution in the third dimension is limited to the slice thickness, and modification of the vessel morphology occurs during decalcification procedures (inhomogeneous tissue shrinkage) and histological slicing (e.g. pleats, folds). Therefore, X-ray tomography techniques can provide complementary information to traditional histology [9].

We have shown that μCT imaging in absorption and phase contrast modes is complementary and invaluable method for studying the morphology and tissue composition of soft and hard tissue-containing human coronary arteries. Synchrotron radiation-based μCT (SRμCT) setups for measurements in absorption contrast mode allow the artery lumen to be segmented while data in phase contrast mode are helpful in the differentiation of the tissue types [9]. For better contrast resolution between soft tissues, SRμCT in phase contrast mode is often used [10]. X-ray phase contrast methods are based on the phase shift of X-ray waves as they pass through the specimen. The shift is related to a change in the real part of the X-ray refractive index. Examples of these methods include propagation based (or *inline*) contrast [11] and phase contrast μCT based on crystal interferometry [12]. Recently, X-ray grating interferometry (XGI) also known as *Talbot interferometry* [13, 14] has become available. This technique uses two gratings placed between the specimen and the detector: the grating closer to the specimen diffracts the incident X-ray beam into the two first diffraction orders with respect to the original direction of propagation. These orders interfere at a certain distance giving a periodic interference pattern that can be analyzed by the second grating [13, 15].

Depending on the type of information required, one or the other imaging techniques is preferred. Here, we address the question of data from atherosclerotic human coronary arteries acquired in phase contrast mode by means of XGI phase SRμCT, and absorption contrast mode acquired by conventional and advanced laboratory μCT. Extracted human coronary arteries are first measured with an advanced μCT setup (nanotom m) in absorption mode to identify plaque-containing regions. Selected parts from each artery are dissected with a scalpel and measured sequentially using a conventional laboratory μCT setup (SkyScan™ 1174) in absorption mode and SRμCT in grating interferometer-based phase contrast mode.

2. MATERIALS AND METHODS

2.1 Multi-modal imaging of atherosclerotic human coronary arteries

Atherosclerotic lesions (*atheromata*) refer to the presence of non-endothelial cells, connective tissue elements and lipids in the innermost layer of the artery [3]. When the lesions increase in size and thickness, blood flow dynamics are altered with respect to the healthy condition and the artery becomes progressively rigid and stenosed. This can lead to a critical situation such as a myocardial infarction due to a near or complete occlusion of the coronary arteries. The morphology of such diseased arteries is of interest for both understanding disease progression and developing possible therapeutic applications.

In this study, the right and left coronary artery trees with vessel diameters of 2 to 6 mm were explanted *post mortem* from 4 % paraformaldehyde (PFA) fixed hearts of three individuals who donated their bodies for teaching and research purposes to the Institute of Anatomy, University of Basel, Switzerland. Extracted arteries were stored in 4 % PFA, in 50 mL Falcon tubes, and measured in their entirety in these containers using advanced laboratory μCT in absorption mode (nanotom m, Phoenix|x-ray, GE Sensing & Inspection Technologies GmbH, Wunstorf, Germany). The reconstructed nanotom images were used to select diseased regions of interest within the specimens, which were cut to the required size with a scalpel and placed in 4 % PFA-filled cylindrical containers with an approximate diameter of

6 mm. These specimens were then measured in phase contrast mode (SRμCT) and absorption mode using a conventional laboratory μCT setup (SkyScan 1174™, Bruker microCT, Kontich, Belgium). To remove air bubbles, each specimen was stored under reduced pressure overnight in a desiccator prior to measurements.

2.2 Conventional laboratory μCT in absorption mode

After measurement of the right and left coronary artery trees using the advanced laboratory μCT setup (nanotom m), three appropriate specimens were subsequently dissected for analysis with a SkyScan 1174™ system (SkyScan, Kontich, Belgium). A maximal acceleration voltage of 50 kV and a beam current of 800 μA were used. The use of a lower maximal acceleration voltage than in the advanced laboratory μCT measurements necessitated the measurement of a smaller field of view and therefore specimen size, since tissue penetration is proportional to X-ray energy. Therefore, individual arteries (9 mm length, 2 to 3 mm diameter) were extracted and measured. The advantage of a smaller field of view is the increase in spatial resolution, making a pixel size of 8.8 μm possible (c.f. subsection 2.3, specimens measured at higher acceleration voltage and larger field of view with consequent pixel size of 33.7 μm, although pixel sizes down to < 1 μm are theoretically possible given a much decreased field of view). 900 projections of 1024 × 1024 pixels were recorded over 360º with an exposure time of 1.2 s per projection. The data were reconstructed by means of the producer's software NRecon, using a modified Feldkamp algorithm, with a correction to reduce ring artifacts.

2.3 Advanced laboratory μCT in absorption mode

The morphology of entire human coronary artery trees (several centimeters in length) was first examined by laboratory μCT with a nanotom m (Phoenix|x-ray, GE Sensing & Inspection Technologies GmbH, Wunstorf, Germany) equipped with a nanofocus X-ray source. An accelerating voltage of 90 kV and a beam current of 200 μA, an exposure time of 1.5 s per projection, and a 0.5 mm-thick Al filter to increase the mean photon energy were used. 1200 projections of 1500 × 2400 pixels were recorded over 360º with a pixel size 33.7 μm. The projections were reconstructed using the cone beam filtered back-projection algorithm available in the phoenix datos|x 2.0.1- RTM software (GE Sensing & Inspection Technologies GmbH, Wunstrorf, Germany).

2.4 Grating interferometer-based phase tomography

SRμCT measurements in grating-based phase contrast mode (XGI-phase SRμCT) were carried out at the beamline P07 (DESY, Hamburg, Germany) operated by the Helmholtz-Zentrum Geesthacht [16]. Figure 1 shows a schematic of the experimental setup used. To reduce artifacts caused by the sharp change in refractive index between the air and container wall, the specimen was placed in a water bath (A). A photon energy of 33 keV was chosen using a double-crystal bent-Laue Si(111) monochromator. The specimen was placed 90 m from the source and 8 cm from g_1 (denoted by B in Figure 1, 4.8 μm periodicity, 16 μm-thick Ni) while g_2 (denoted by C in Figure 1, 2.4 μm periodicity, 120 μm-thick Au) was at 23 cm (third fractional Talbot order) from the first grating. The X-ray detector unit consisted of a luminescent screen made of $CdWO_4$, optical lens and CCD camera. The incident X-ray beam was converted into visible light by the luminescent screen, projected with a magnification of 5.00 onto the CCD camera. 500 projections were taken over a range of 360º with an exposure time of 0.8 s per phase step. For each projection angle, four phase-stepping images were recorded over one period of the interference pattern. The effective pixel size corresponded to 2.4 μm and the field of view was 2 mm × 7 mm. More details about grating interferometry and the phase stepping method can be found in Weitkamp et al. [15]. The datasets from the phase contrast projections were reconstructed using a modified filter kernel (Hilbert transform) in combination with a standard filter back-projection algorithm [17, 18]. To avoid strong ring artifacts and improve the quality of reconstructed images, a *wavelet-Fourier* filter was applied [19].

The XGI-phase SRμCT slice presented in Figure 6 was part of a measurement carried out at the beamline ID19 (ESRF, Grenoble, France). A photon energy of 53 keV was chosen using a double-crystal Si(111) monochromator. The specimen was placed 11.5 cm from g_1 (4.8 μm periodicity, 11 μm-thick Ni) while g_2 (2.4 μm periodicity, 100 μm-thick Au) was at a distance of 36.7 cm from the first grating (ninth fractional Talbot order) and 10.5 cm from the detector. The X-ray detector unit comprised a $CdWO_4$ luminescent screen, optical lens and CCD camera with a pixel size of 7.5 μm. 999 projections were taken over a range of 360º with an exposure time of 2 s per phase step. For each projection angle, four phase-stepping images were recorded over one period of the interference pattern. The effective pixel size corresponded to 5.18 μm with a field of view of 4.7 mm × 10.6 mm.

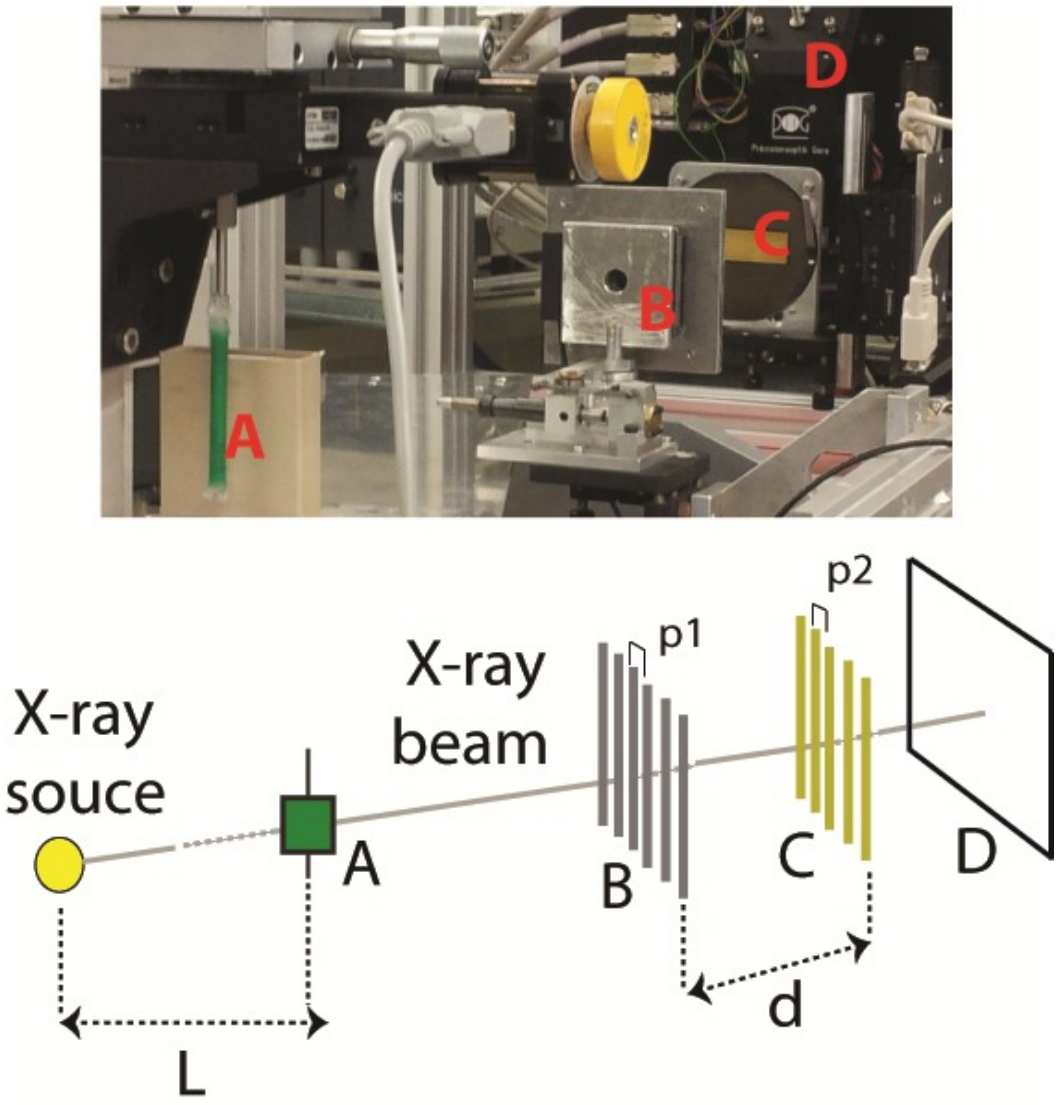

Figure 1. Photograph and schematic of the grating interferometer setup for tomographic imaging: A) specimen, B) phase grating g_1, C) analyzer grating g_2, and D) detector. The distance between the two gratings (d) was 23 cm (third fractional Talbot order). The specimen distance from the X-ray source (L) was 90 m.

2.5 Histology

In order to prepare histological sections, a portion of one human coronary artery was decalcified and embedded in paraffin. The artery was immersed in decalcifier (distilled water : formic acid : PFA, 87 : 8 : 5 v/v) at a temperature of 37 °C for two days. Subsequently, it was dehydrated by sequential soaking in alcohol then xylene overnight at reduced pressure (Tissue-Tek VIP E300 Histokinetic automated dehydrator, Sakura) and immersed in molten paraffin at a temperature of 60 °C. The paraffin was allowed to cool and the block was trimmed with a scalpel to the size of the artery-containing region. Histological sections of 2 to 4 μm thickness were cut (Microm Cool-cut HYRAX M 40, Carl Zeiss), stained with hematoxylin and eosin (H&E) stain and mounted on glass slides. Each slice was photographed using a Nikon Eclipse 80i microscope and camera at 10× magnification in an average of 20 sections and stitched together using the stitching plug-in [20] available in the Fiji software (ImageJ version 1.45k, EMBL, Germany) [21]. This gave color images of an average of 4500 × 5500 pixels (0.5 × 0.5 μm^2) that were binned to reduce the size of the dataset for ease of handling, and converted to gray scale images for further analysis.

3. RESULTS

3.1 Advanced laboratory μCT for identifying plaque and soft tissues in human coronary arteries

Three arteries were first measured using conventional (absorption contrast) laboratory μCT with a nanotom m (Phoenix|x-ray, GE Sensing & Ispection Technologies GmbH, Wunstorf, Germany). Human coronary artery trees were visualized in their entirety. The reconstructed 3D data of the three arteries measured using this imaging modality were visualized and segmented using the thresholding tool in VG Studio Max 2.1 (Volume Graphics, Heidelberg, Germany). Such thresholding allowed the plaques to be easily segmented from the soft tissues (Figure 2, top). The white arrows in the 3D plaque images indicate the position of the corresponding 2D slice showing the artery cross section (Figure 2, bottom). The plaque, lumen, smooth muscle and surrounding soft tissue are clearly visible. From the reconstructed images, 8 mm sections with significant plaque occlusions were selected for the subsequently performed SRμCT measurements.

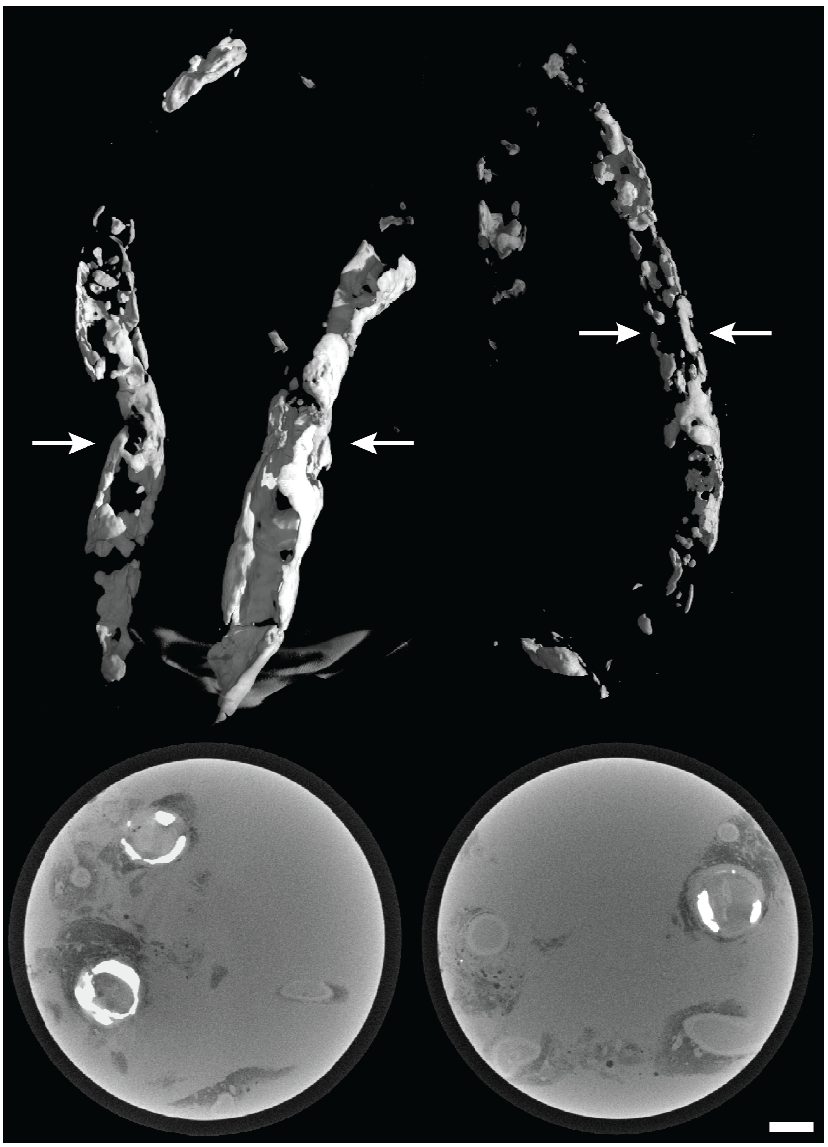

Figure 2. 3D renderings of plaques on the two human coronary artery trees (top) with white arrows indicating the related 2D slices (bottom). In the 2D slices, the white part shows the plaques, while the dark grey part corresponds to surrounding muscle and light grey corresponds to the vessel walls. The scale bar corresponds to 3 mm.

3.2 Ring artifact correction with a wavelet-Fourier filter

In order to improve the quality of reconstructed phase-contrast SRμCT slices, particularly with respect to high-frequency ring artifacts overlaying small features of the sample and impeding segmentation, a wavelet-Fourier stripe filtering technique was applied to the sinograms before reconstruction [19]. Figure 3 compares a slice obtained from one of the arteries reconstructed from the unfiltered data (left) to a slice reconstructed from the wavelet-Fourier filtered sinogram (right). The filter parameters were chosen to be: highest decomposition level $L = 6$; wavelet type, db25; damping factor $\sigma = 3.0$. On visual inspection, the ring artifacts, in particular the high-frequency ones were mostly removed while all features of the sample were retained. Only towards the edges of the container did broad, but weak, low-frequency rings become visible. Line profiles of the $\Delta\delta$ values through the specimen (not shown) confirmed that all features, and steepness of changes between features, were well retained.

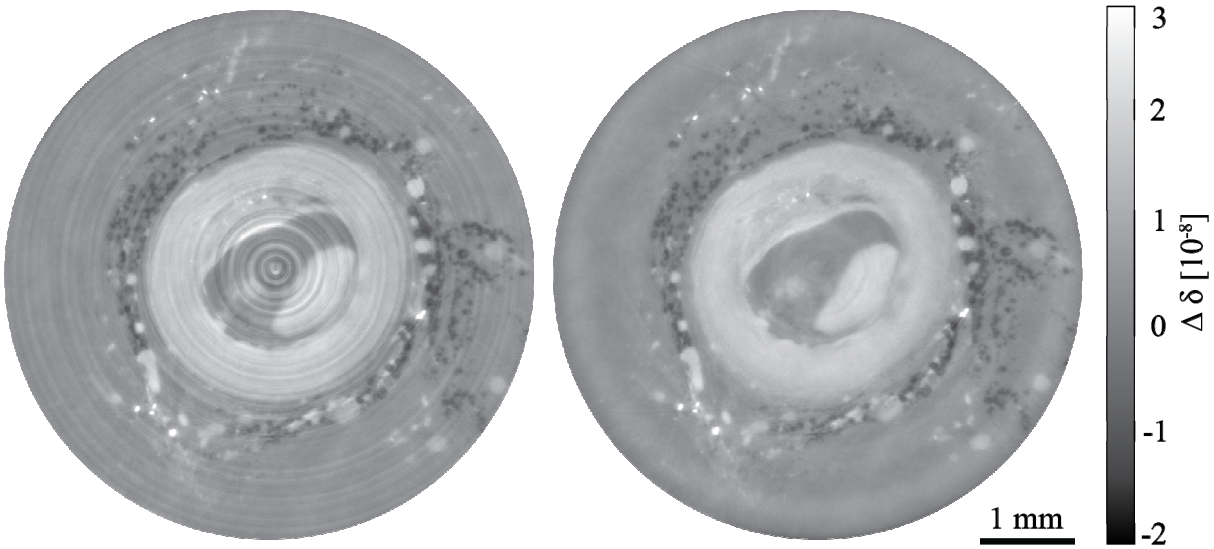

Figure 3. Human coronary artery slices from SRμCT in phase contrast mode: unfiltered data (left) and data corrected using wavelet-Fourier filtering (right). A decrease in ring artifact effects is clearly visible (measurement performed at beamline P07, DESY, Hamburg, Germany).

3.3 Extracting lumen morphology using XGI-phase SRμCT

Figure 4 shows the reconstructed data of one of the arteries measured using XGI-phase SRμCT at beamline P07 (DESY, Hamburg, Germany) with the sinograms pre-processed using the wavelet-Fourier filter before reconstruction as demonstrated in Figure 3. The effective lumen area available for blood flow (yellow part, top right and bottom left) was segmented from the three-dimensional data using a region-growing algorithm available in VG Studio Max 2.1 (Volume Graphics, Heidelberg, Germany). The cross-sectional area for each reconstructed slice was calculated and found to vary from a maximum of 3.26 mm^2 to a minimum of 1.09 mm^2, corresponding to a 66.5 % stenosis by cross-sectional area along the 8 mm artery section (cp. Figure 4, bottom, right). One slice shown as an example in Figure 4 is taken at the position 2.7 mm along the artery and indicated by the dashed red line in Figure 4, bottom right.

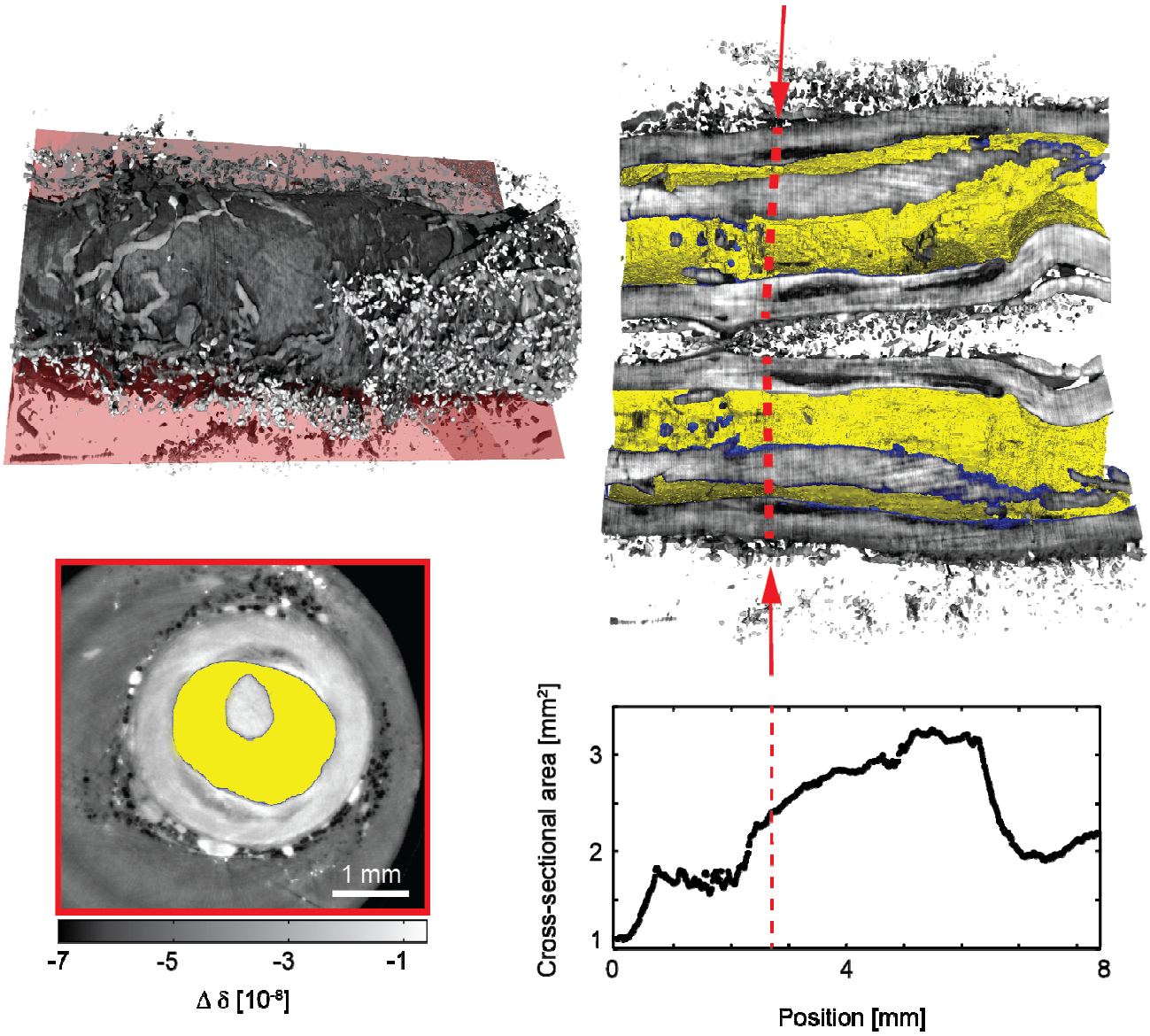

Figure 4. 3D representation of the soft tissues of a section of a selected artery (top left) and cross-sectional representation of the same artery (top right) showing the lumen morphology (yellow). A 2D slice from the same artery (bottom left) shows the area available for blood flow (yellow), vessel wall (light grey) and surrounding tissues (white and dark grey spots). The cross-sectional area plot (bottom right) shows how the non-constricted lumen area available for blood flow changes along the length of the dissected artery directly above it. Each point corresponds to one slice.

3.4 Comparison of XGI-phase SRμCT with conventional laboratory μCT

Three-dimensional data from XGI-phase SRμCT and conventional laboratory μCT of the human coronary artery were rigidly registered. Figure 5 shows the histograms of the entire datasets from both acquisitions. XGI-phase SRμCT data gives the most information about tissue composition: the five peaks in the histogram of the three-dimensional dataset correspond to the $\Delta\delta$ values of distinguishable soft tissues (Figure 5, top right). The peaks are sufficiently distinct that intensity-based segmentation with a threshold can be used to extract information about tissue types. However, the histogram from the conventional laboratory μCT data contains only two peaks, corresponding to the vessel wall-

comprising tissues and surrounding muscle. Visual distinction of tissue types in the related two-dimensional slice is also greatly restricted in comparison to the phase contrast. With the lumen barely visible but clearly resolved white and darker spots one find indications of plaque and the surrounding muscle, respectively, on the exterior of the artery wall (Figure 5, left side).

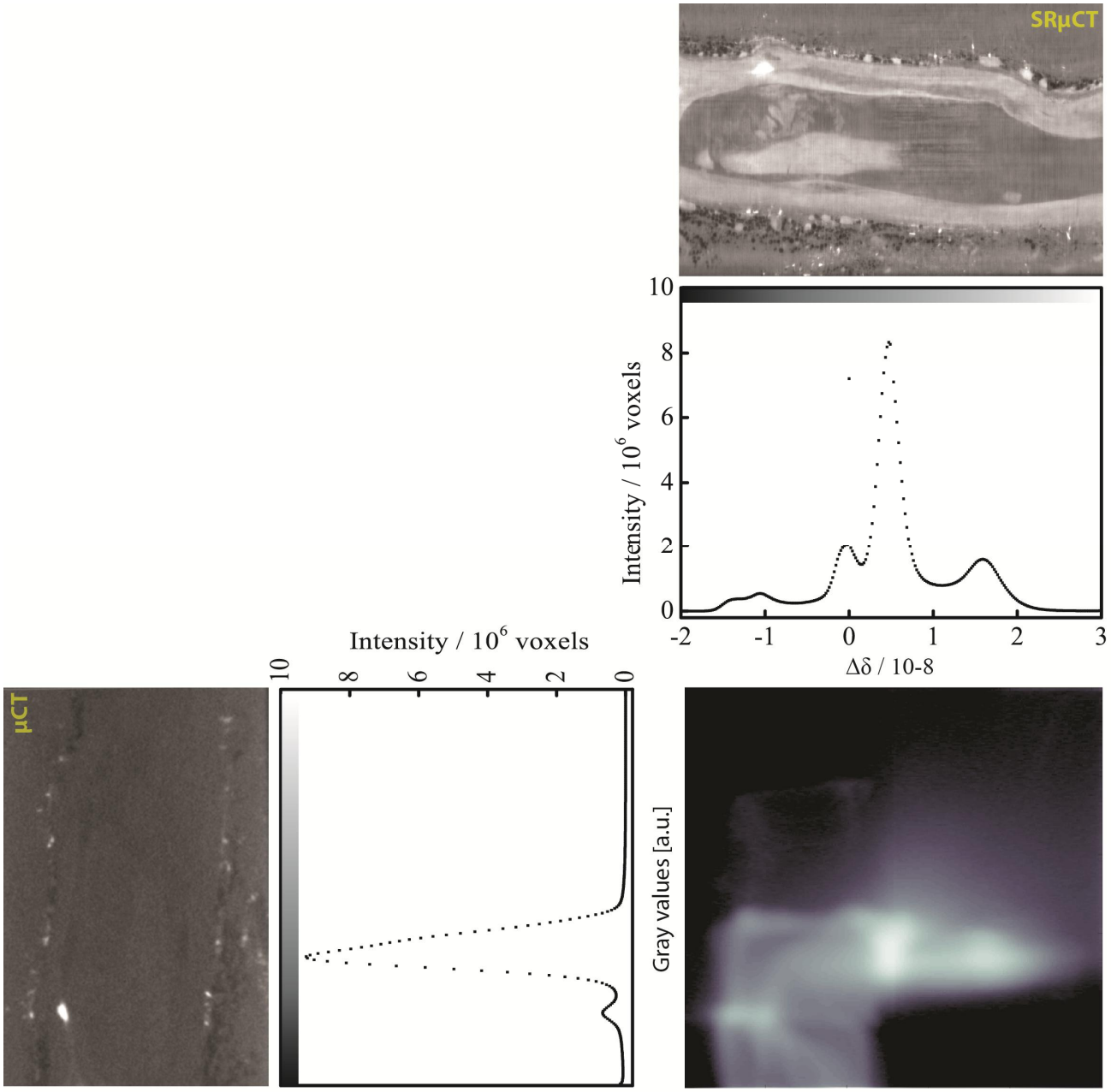

Figure 5. Comparison between XGI-phase SRμCT (top, right) and conventional laboratory μCT (bottom, left) illustrated in the joint histogram (bottom, right).

The joint histogram [22] of the 3D reconstructed datasets (Figure 5, bottom right) shows how the combination of the two techniques allows more information to be extracted from the combined measurements than is possible by simply examining each dataset individually. Although most of the distinguishable peaks in the XGI phase SRμCT are contained within the larger conventional laboratory μCT peak, the peaks with $\Delta\delta$ values around -1 to -2×10^{-8} can be attributed to

both the right edge of the large conventional laboratory μCT histogram peak and the smaller peak to the left. By highlighting the tissues that contribute to these peaks in both 3D datasets using intensity-based segmentation with a threshold, it is possible to identify differences in the tissues corresponding to these peaks by comparing the two datasets [8, 23].

3.5 Rigid registration of a human coronary artery slice using histology and SRμCT data

Correspondence between two-dimensional histological slices and three-dimensional SRμCT data was established using a recently proposed algorithm for automatic 2D-3D matching [23]. This algorithm is based on scale and rotation invariant feature detector SURF [24] and density-driven RANSAC [25]. At first, it computes corresponding feature points between a gray scale histological image and each image in the SRμCT volumetric data with their associated coordinates. These coordinates are sequentially stored in a 3D point cloud, where the third dimension corresponds to the slice number in the SRμCT data. Then, the plane that best matches the histological image is extracted from the noisy 3D feature point cloud using a modified RANSAC algorithm. The main advantage of RANSAC is that it can robustly detect a plane with the highest point density in a dataset with many outliers. The last step reduces to an interpolation of a 2D image from the SRμCT dataset based on the estimated plane parameters.

Furthermore, the histology slice was rigidly registered to the SRμCT slice generated from 2D-3D matching in MatLab R2012b (The MathWorks, Natick, USA) using rigid body 2D image co-registration (translation and rotation) by maximization of mutual information [26, 27]. Although the registered data (Figure 6) is of interest for visual inspection, it is not of sufficient quality to allow for the non-rigid registration, necessary for a quantitative evaluation of tissue types using a joint histogram [23].

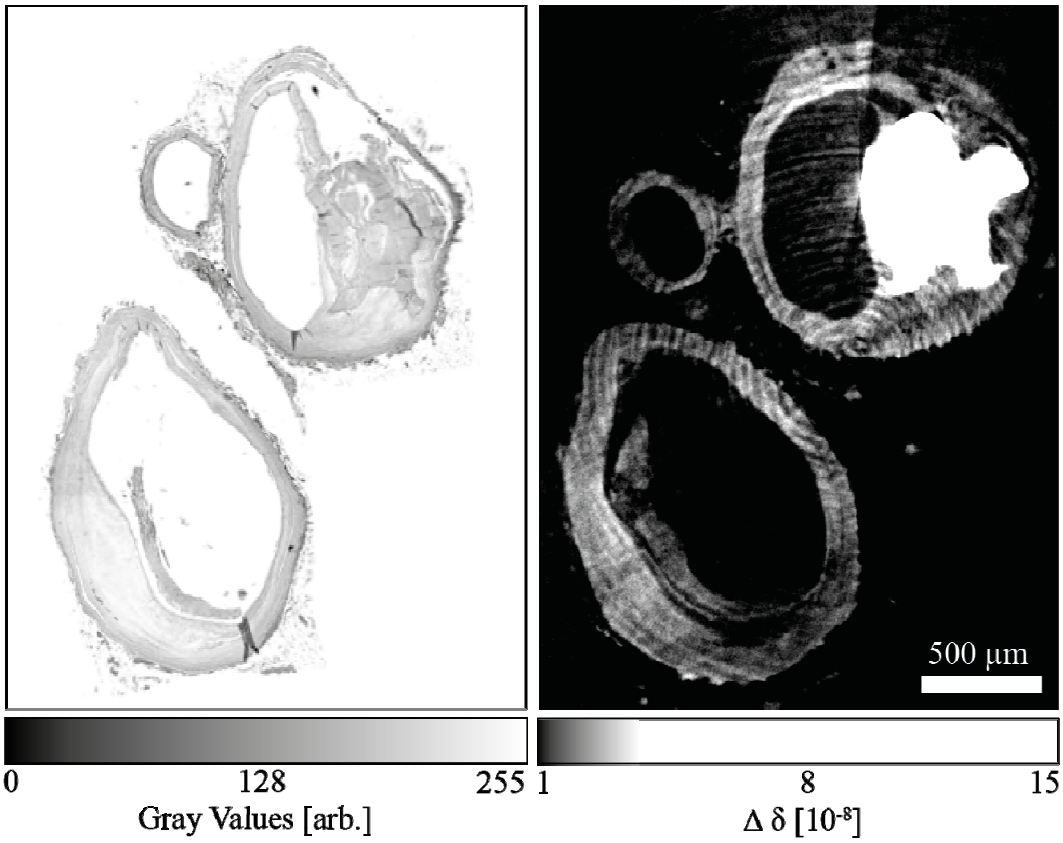

Figure 6. Gray-scale image of a decalcified histological slice stained with hematoxylin and eosin stain (left) and corresponding calcified XGI-phase SRμCT slice generated by automatic 2D-3D matching (right). The histological slice has been rigidly registered to the XGI-phase SRμCT slice on the right (measurement performed at beamline ID19, ESRF, Grenoble, France).

4. DISCUSSION

4.1 Advanced laboratory μ-CT for identifying plaque and soft tissues in human coronary arteries

Advanced laboratory μCT is an invaluable tool for measuring the three-dimensional morphology of soft and hard tissues containing biological specimens, e.g. atherosclerotic human coronary arteries. One of the main advantages of this technique over the XGI-phase SRμCT setups discussed here is the size of sample that can be measured in a rather fast fashion. SRμCT measurements are restricted to several millimeters in height by the X-ray beam height and beamline setups reported here. However, in the advanced laboratory μCT protocol presented here, specimens of several centimeters in diameter and height can be measured and the data can be reconstructed within a period of 6 to 8 h. Therefore, it is feasible to screen several specimens and, using e.g. segmentation of the plaque from reconstructed data, select specific regions of interest before subsequent more sophisticated and costly SRμCT measurements.

In addition to information about the location and quantity of plaque, the vessel lumen morphology is of great interest for extracting a lumen mesh that can be used for blood flow simulations. However, intensity-based thresholding and region-growing segmentation cannot be used to segment the vessel wall in the advanced laboratory μCT datasets presented here (see Figure 2), due to overlapping grey values of the lumen and formalin. Additionally, a larger field of view comes at the cost of decreased spatial resolution, with pixel sizes in the tens of microns (although given a minimal field of view pixel sizes of < 1 μm are theoretically possible with this imaging modality). Therefore, complementary imaging techniques are essential to gather such data.

4.2 Ring artifact correction with a wavelet-Fourier filter

The wavelet-Fourier filtering procedure allows dampening of high-frequency ring artifacts so that detailed features both inside the artery as well as in the artery wall are revealed and retained, and further analysis, e.g. through lumen segmentation, is facilitated. Applying a wavelet-Fourier filter to the sinograms before data reconstruction was extremely effective in removing ring artifacts, with negligibly weak effects on small features. In their original paper, Münch et al. [19] claim that, aside from an effective energy loss due to the filtering, a windmill-like twist of the inner region might occur in some cases. Tracking the positions of selected small features inside the artery, we have ensured that the filter parameters were chosen so that such an effect did not arise or was kept negligibly weak. Even though the artery is almost concentric with the ring artifacts to be removed, the wavelet filter did not affect the morphology of the artery. This is a powerful tool for data treatment that greatly improves the quality of subsequent data analysis.

4.3 Extracting lumen morphology using XGI-phase SRμCT

Although it was impossible here to extract information about the lumen morphology from advanced and conventional laboratory μCT, is was possible with XGI-phase SRμCT data, in which the sinograms had been pre-processed with a wavelet-Fourier filter. The 66.5 % stenosis identified in the artery presented here is not what one might consider as *critically stenosed*, i.e. > 80 % occlusion by cross sectional area [28], although still relevant for understanding the morphology and tissue composition of atherosclerotic arteries during disease progression. Although we have previously extracted the vessel lumen from decalcified arteries [9], this is the first example of extracting the lumen form a calcified human coronary artery. The lumen extraction was made possible in part by the application of the wavelet-Fourier filter to the sinograms before data reconstruction, to remove the numerous more or less pronounced ring artifacts.

4.4 Comparison of XGI-phase SRμCT with conventional laboratory μCT

We have shown previously that the combination of datasets acquired using complementary imaging modalities can lead to identification of tissue types not possible by each modality alone, e.g. the combination of XGI-phase SRμCT, μMRI and histology to distinctly segment the stratum granulosum, stratum moleculare, white matter, and brain tissue in human brain [8]. Here too, there is some added value in combining the results from conventional laboratory μCT with the XGI phase SRμCT. Although the tissue contrast in conventional laboratory μCT dataset image is vastly inferior to that of the XGI-phase SRμCT, combining the two datasets in a joint histogram allows information about tissue composition to be extracted that is impossible by considering the two datasets independently.

4.5 Rigid registration of a human coronary artery slice using histology and SRμCT data

Histology is recognized as the gold standard for visualizing biological tissues. The spatial resolution within the plane reaches the sub-micrometer level and is usually limited to the wavelength of light. Several stains exist for identifying specific cell and connective tissue types. However, the spatial resolution in the third dimension is limited by the cutting

slice thickness to values of for example 2 to 5 μm and it is time-consuming to prepare and stack slices for a three-dimensional dataset several centimeters in height. Additionally, invasive steps required before slicing (decalcification, paraffin embedding) can lead to heterogeneous strain on specimens and modifications in the morphology, and cutting itself induces artifacts such as pleats and folds in the individual slices. When accurate data about the specimen morphology is required, multi-modal images are needed as complementary approach.

The identification of the position of a histology slice within the tomography dataset was made possible by an automatic registration tool, previously used in the evaluation of the regenerative capacity of bone grafting materials [23]. However, in the example of human coronary arteries presented here, the registration between the phase SRμCT data set and the histological slices is very challenging mainly due to two reasons. First, very little of the surrounding muscle tissue is included in the images of the histological slices of the arteries. Therefore, it was necessary to remove surrounding muscle from the SRμCT data by thresholding. This method however was not ideal and the presence of some surrounding muscle tissue in the histology slices caused problems during the non-rigid registration. Second, the histological slice has deformities such as pleats and folds that are a result of the slicing. Although our rigid 2D-3D registration approach was able to identify a reasonable CT-slice for one histological slice as shown in Figure 6, a non-rigid registration, a requirement for a joint histogram, remains elusive.

5. CONCLUSIONS

XGI-phase SRμCT is an invaluable tool for uncovering information about soft and hard tissues containing specimens, e.g. diseased human coronary arteries as shown in this study. Their combination with other techniques such as conventional and advanced μCT and histology can allow still more information to be extracted from the datasets.

We have previously reported [28] that XGI-phase SRμCT data is preferential for identifying soft tissues within a decalcified artery, while conventional absorption-based SRμCT is better suited for the extraction of the lumen morphology. Here, we show that by using a higher energy X-ray beam and calcified human coronary arteries it is possible both to extract the lumen morphology (cp. Figure 4) and to identify soft tissue types (Figure 5) within the same dataset. This was in part due to additional pre-processing of the sinograms before data reconstruction using a wavelet-Fourier filter to remove ring artifacts.

If the obstacles to non-rigid registration of histology and XGI-phase SRμCT can be overcome, joint histograms of these imaging modalities would allow comparison of our findings with the medical gold standard of two-dimensional imaging.

ACKNOWLEDGEMENTS

This work was primarily funded by the Swiss National Science Foundation (SNSF) in the National Research Program (NRP) 62 ‘Smart Materials’ framework within the project number 406240_126090 ‘NO-Stress’ and via SNSF Division II - Mathematics, Natural sciences and Engineering within the grant 205321_150164: *Multi-modal matching of two-dimensional images with three-dimensional data in the field of biomedical engineering* (Information Sciences). Synchrotron radiation beamtime from the ESRF and the HASYLAB at DESY is gratefully appreciated. We thank M. Müller-Gerbl of the Department of Anatomy, University of Basel, who provided the human arteries and the team of J. A. Lobrinus of the Department of Clinical Pathology, University Hospitals of Geneva for preparing the artery histological slices. We are grateful to J. Mohr and his collaborators at the Institute for Microstructure Technology (IMT) of KIT, Karlsruhe, Germany for providing the analyzer grating. We also thank A. Zumbuehl and A. Weinberger of the Department of Chemistry, University of Fribourg, Switzerland and V. Kurtcuoglu of the Institute of Physiology, University of Zurich, Switzerland for stimulating discussions concerning mechano-sensitive drug delivery and blood flow simulations using meshes extracted from human coronary arteries in the diseased state.

REFERENCES

[1] Kivimaki, M., Nyberg, S.T., Batty, G.D*., et al.*, "Job strain as a risk factor for coronary heart disease: A collaborative meta-analysis of individual participant data," Lancet **380** (9852), 1491-1497 (2012).

[2] Lee, I., Shiroma, E.J., Lobelo, F*., et al.*, "Impact of physical inactivity on the world’s major non-communicable diseases," Lancet **380** (9838), 219-229 (2012).

[3] Hansson, G.K., "Inflammation, Atherosclerosis, and Coronary Artery Disease," N. Engl. J. Med. **352**, 1685-1695 (2005).
[4] Saxer, T., Zumbuehl, A., and Müller, B., "The use of shear stress for targeted drug delivery," Cardiovasc. Res. **99** (2), 229-231 (2013).
[5] Wellnhofer, E., Osman, J., Kertzscher, U.*, et al.*, "Non-dimensional modeling in flow simulation studies of coronary arteries including side-branches: A novel diagnostic tool in coronary artery disease," Atherosclerosis **216** (2), 277-282 (2011).
[6] Mellal, D. and Zumbuehl, A., "Exit-strategies – smart ways to release phospholipid vesicle cargo," J. Mater. Chem. B **2**, 247-252 (2014).
[7] Holme, M.N., Fedotenko, I.A., Abegg, D.*, et al.*, "Shear-stress sensitive lenticular vesicles for targeted drug delivery," Nat. Nanotech. **7** (8), 536-543 (2012).
[8] Schulz, G., Waschkies, C., Pfeiffer, F.*, et al.*, "Multimodal imaging of human cerebellum - merging X-ray phase microtomography, magnetic resonance microscopy and histology," Sci. Rep. **2**, 826 (2012).
[9] Holme, M.N., Schulz, G., Deyhle, H.*, et al.*, "Complementary X-ray tomography techniques for histology-validated 3D imaging of soft and hard tissues using plaque-containing blood vessels as examples," Nat. Protoc. **9** (6), 1401-1415 (2014).
[10] Fitzgerald, R., "Phase-Sensitive X-Ray Imaging," Phys. Today **53** (7), 23-26 (2000).
[11] Snigirev, A.A., Snigireva, I., Kohn, V.*, et al.*, "On the possibilities of X-ray phase contrast microimaging by coherent high-energy synchrotron radiation," Rev. Sci. Instrum. **66** (12), 5486–5492 (1995).
[12] Bonse, U. and Busch, F., "X-ray computed microtomography (μCT) using synchrotron radiation (SR)," Prog. Biophys. Mol. Bio. **65** (1-2), 133-169 (1996).
[13] David, C., Nöhammer, B., Solak, H.H.*, et al.*, "Differential phase-contrast imaging using a grating interferometer," Appl. Phys. Lett. **81**, 3287-3289 (2002).
[14] Momose, A., Kawamoto, S., Koyama, I.*, et al.*, "Demostration of X-ray Talbot interferometry," Jpn. J. Appl. Phys., Part 2 **42** (7B), 866-868 (2003).
[15] Weitkamp, T., Diaz, A., David, C.*, et al.*, "X-ray phase imaging with a grating interferometer," Opt. Express **13** (16), 6296-6304 (2005).
[16] Hipp, A., Beckmann, F., Lytaev, P.*, et al.*, "Grating-based X-ray phase-contrast imaging at PETRA III," Proc. SPIE **9212**, 9212-5 (2014).
[17] Faris, G.W. and Byer, R.L., "Three-dimensional beam-deflection optical tomography of a supersonic jet," Appl. Optics **27** (24), 5202-5212 (1988).
[18] Pfeiffer, F., Bunk, O., Kottler, C.*, et al.*, "Tomographic reconstruction of three-dimensional objects from hard X-ray differential phase contrast projection images," Nucl. Instrum. Meth. A **580** (2), 925-928 (2007).
[19] Münch, B., Trtik, P., Marone, F.*, et al.*, "Stripe and ring artifact removal with combined wavelet — Fourier filtering," Opt. Express **17** (10), 8567-8591 (2009).
[20] Preibisch, S., Saalfeld, S., and Tomancak, P., "Globally optimal stitching of tiled 3D microscopic image acquisitions," Bioinformatics **25** (11), 1463-1465 (2009).
[21] Walter, T., Shattuck, D.W., Baldock, R.*, et al.*, "Visualization of image data from cells to organisms," Nat. Methods **7** (6), 479-479 (2010).
[22] Müller, B., Deyhle, H., Lang, S.*, et al.*, "Three-dimensional registration of tomography data for quantification in biomaterials science," Int. J. Mat. Res. **103** (2), 242-249 (2012).
[23] Stalder, A.K., Ilgenstein, B., Chicherova, N.*, et al.*, "Combined use of micro computed tomography and histology to evaluate the regenerative capacity of bone grafting materials," Int. J. Mat. Res. **105** (7), 679-691 (2014).
[24] Bay, H., Ess, A., Tuytelaars, T.*, et al.*, "Speeded-up robust features (SURF)," Comp. Vis. Imag. Und. **110** (3), 346-359 (2008).
[25] Fischler, M.A. and Bolles, R.C., "Random sample consensus: A paradigm for model fitting with applications to image analysis and automated cartography," Commun. ACM **24** (6), 381-395 (1981).
[26] Flannery, B.P., Teukolsky, S.A., and Vetterling, W.T., [Numerical Recipes, The Art of Scientific Computing], W.H. Press (1986).
[27] Lu, X., Zhang, S., Su, H.*, et al.*, "Mutual information-based multimodal image registration using a novel joint histogram estimation," Comput. Med. Imag. Graph. **32** (3), 202-209 (2008).
[28] Holme, M.N., Schulz, G., Deyhle, H.*, et al.*, "Morphology of atherosclerotic coronary arteries," Proc. SPIE **8506**, 850609 (2012).